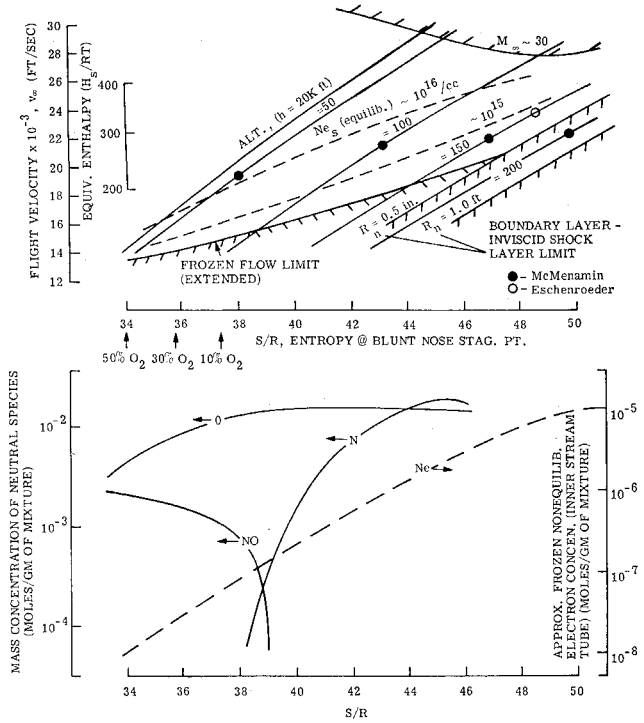

Fig. 4 Correlation and prediction of shock layer properties as a function of flight conditions.

bols) at this body station for the four flight conditions as compared to the composition based on the nozzle entropy correlation (solid lines).[1,2] The species considered are O_2, N_2, O and N. With the exception of the order of magnitude disagreement between the calculated value of N and the value for N predicted by the correlation at the 50-k ft condition, the overall agreement is quite good, and the correlation appears to predict the chemical properties in the frozen nonequilibrium portion of the inviscid center body stream tube quite well.

Figure 4 presents the entropy correlation of shock layer flow properties as a function of vehicle flight conditions. Flight velocity (v_∞) and center body stream tube stagnation point enthalpy (H_s/RT_0) are presented vs entropy (S/R). Lines of constant flight altitude (h) and stagnation point electron density [$Ne_{s(\text{equilib.})}$] are also included. The four flight conditions that were used are shown (filled circles) as well as the flight point from Ref. 11 (open circle).[4] The altitude boundaries for achieving a viscous boundary-layer inviscid shock layer flow are presented for both a 0.5 in. and 1.0-ft nose radius center body. The other limit line is the frozen line.[2,4,7] Presented below the flight condition plot in Fig. 4 is a replot of the entropy correlation of neutral species and electron concentration. One need only to use the top half of Fig. 4 to determine the stagnation point entropy value at any given point on a flight trajectory (v_∞ and h). Then, by projecting straight down along this entropy value to the curves below, an estimate of the electron concentration is obtained as well as fairly accurate quantitative values of the neutral chemical species concentration. Thus, for example, a vehicle at 100-k ft altitude and flying at 25,000 fps is predicted to have a downstream center body stream tube electron density value of 3×10^{-6} (mol/g mix.) and the neutral chemical species composition specified at the entropy (S/R) value of 46. The stagnation point equilibrium electron density value will be 10^{16} electrons/cm^3.

The applicability of this shock layer prediction technique is as shown in Fig. 4. Therefore, the prediction technique is generally applicable from h = 200-k ft for v_∞ between 22 to 33-k fps to h = 50-k for v_∞ between 12-k fps to 30-k fps.

References

[1] Harris, C. J., "Comment on Nonequilibrium Effects on High-Enthalpy Expansion of Air," *AIAA Journal*, Vol. 4, No. 6, June 1966, pp. 1148–1149.

[2] Harris, C. J. and Warren, W. R., "Correlation of Nonequilibrium Chemical Properties of Expanding Air Flows," R64SD92, Dec. 1964, General Electric Co., Valley Forge, Pa.

[3] Harris, C. J., Marston, C., and Warren, W. R., "MHD Generator and Accelerator Experiments in Seeded and Unseeded Air Flows," R66SD50, Sept. 1966, General Electric Co., Valley Forge, Pa.

[4] Harris, C. J., "Correlation of Inviscid Air Nonequilibrium Shock Layer Properties," R68SD333, Dec. 1968, General Electric Co., Valley Forge, Pa.

[5] Harney, D. J., "Similarity of Nonequilibrium Expansions in Hypersonic Nozzles," FDM-TM-67-1, May 1967, Wright-Patterson Air Force Base, Ohio.

[6] Ring, L. E. and Johnson, P. W., "Correlation and Prediction of Air Nonequilibrium in Nozzles," AIAA Paper 68-378, San Francisco, Calif., 1968.

[7] Marston, C. H. and Warren, W. R., "Study of a Continuous Discharge Driver/Non-Reflected/Free Piston Shock Tunnel," *AIAA Journal*, Vol. 7, No. 5, May 1969, pp. 964–967.

[8] Warren, W. R. and Harris, C. J., "A Critique of High-Performance Shock Tube Driving Techniques," TR-0066 (5240-10)-6, Sept. 1969, Aerospace Corp., El Segundo, Calif.

[9] Leonard, R. L. and Rose, P. H., "Feasibility of a High Performance Aerodynamic Impulse Facility," *AIAA Journal*, Vol. 6, No. 3, March 1968, pp. 448–457.

[10] McMenamin, D. and O'Brien, M., "The Finite Difference Solution of Multicomponent Nonequilibrium Steady Influscid Stream Tube Flows Using a Novel Stepping Technique," 67SD-241, April 1967, General Electric Co., Valley Forge, Pa.

[11] Eschenroeder, A. Q., "Ionization Nonequilibrium in Expanding Flows," *ARS Journal*, Vol. 31, No. 2, Feb. 1961, pp. 196–203.

Amplification by Wave Distortion in Unstable Combustors

M. F. Heidmann*

NASA Lewis Research Center, Cleveland, Ohio

Nomenclature

C_1	=	proportionality constant
c	=	speed of sound
D	=	drop diameter
n	=	harmonic order
P'	=	pressure perturbation
p_1,p_2	=	harmonic coefficients for P'
Re	=	Reynolds number of drop
$\Re$	=	response (burning rate perturbation in-phase with pressure oscillation) described by Eq. (5)
t	=	time
U	=	magnitude of relative drop velocity vector
u_l	=	axial velocity of drop
u_z,u_θ,u_r	=	gas velocity in axial, tangential and radial directions
W,W'	=	normalized drop burning rate (actual and perturbation)
w,w_0	=	drop burning rate (actual and initial value)
γ	=	ratio of specific heats
$\rho,\bar{\rho},\rho'$	=	gas density (actual, mean value and perturbation)
φ_2	=	phase relation between first and second harmonic components
φ_u	=	phase relation between pressure and acoustic particle velocity
μ	=	gas viscosity

Received September 2, 1970; revision received October 15, 1970.

* Aerospace Scientist. Member AIAA.

ω = frequency
ΔV = relative axial velocity of drop
$(\ )'$ = dimensionless perturbations, $x' = (x - \bar{x})/\bar{x}$

Introduction

ACOUSTIC mode instability in rocket and jet engines almost invariably exhibits some type of wave distortion (pressure waves which depart from pure sinusoidal forms). In this Note, a brief analysis is presented that shows engine stability to be highly dependent on this distortion—even when the distortion is small and seemingly negligible.

The analysis is based on a combustion model where burning rate is simply related to a Reynolds number to the one-half power. As such, the model generally represents the convective heat or mass transfer processes but, in this study, drop vaporization in liquid propellant rocket combustors is of specific interest. During steady combustion, the burning rate in liquid rockets is usually vaporization limited. Unsteady combustion is also expected to depend on the vaporization process. Dynamic analysis of the vaporization process with pure sinusoidal wave shapes,[1,2] however, shows an acoustic gain which is insufficient to overcome acoustic losses.

Priem and Guentert[3] using a simple vaporization process—burning rate proportional to the one-half power of Reynolds number—showed, by nonlinear numerical analysis, that a finite perturbation produced instability. Examining the detailed numerical computations reveals a property that is very important in instability. Distorted acoustic oscillations are always generated. Although a sinusoidal disturbance is initially introduced, this property is quickly lost and the disturbance develops into a distorted waveform.

Analysis

The open-loop response of the combustion process will be calculated to predict the acoustic amplification of the process within an unstable combustor. In such open-loop analysis, the perturbations in burning rate caused by assumed acoustic oscillations are calculated.

The burning rate is assumed to be given by

$$w = c_1(Re)^{1/2} = c_1(D\rho U/\mu)^{1/2} \tag{1}$$

This simulates vaporization limited combustion when convective heat transfer to the drop dominates the rate process.

For an axially moving drop in a cylinder, U is the magnitude of a relative velocity vector defined by

$$U^2 = (u_l = u_z)^2 + u_\theta^2 + u_r^2 \tag{2}$$

For this analysis $u_l - u_z$, μ and D are assumed constant and u_r is neglected. These assumptions basically restrict the results to high frequencies or large drops and to transverse oscillations in a cylinder. The same assumptions were originally used by Priem and Guentert in Ref. 3.

Defining the gas density as $\rho = \bar{\rho}(1 + \rho')$, a nondimensional burning rate, W, can be expressed as

$$W = w/w_0 = (1 + \rho')^{1/2}[1 + (\mu_\theta/\Delta V)^2]^{1/4} \tag{3}$$

where

$$w_0 = c_1(\bar{\rho}D\Delta V/\mu)^{1/2},\ \Delta V = |u_l - u_z|$$

Acoustic waves distorted by second harmonic content are assumed to be approximated by

$$P' = p_1 \cos\omega t + p_2 \cos(2\omega t - \varphi_2)$$

$$\rho' = (1/\gamma)[p_1 \cos\omega t + p_2 \cos(2\omega t - \varphi_2)]$$

$$u_\theta = (c/\gamma)[p_1 \cos(\omega t - \varphi_u) + p_2 \cos(2\omega t - \varphi_2 - \varphi_u)] \tag{4}$$

These relations allow for a variable amount of second harmonic content and a variable phase relation (φ_2) between the first and second harmonics. Depending upon the acoustic mode, particle velocities can vary from an in-phase to an out-of-phase relation with the pressure oscillation. The velocity phase angle φ_u allows for this variation.

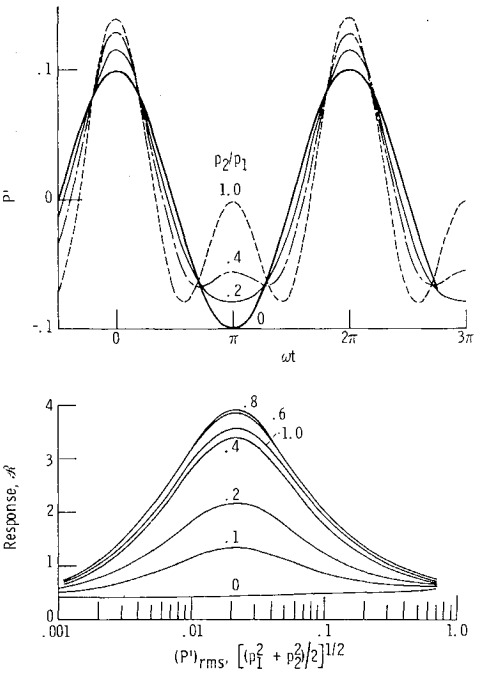

Fig. 1 Effect of amount of harmonic content on response. $\varphi_2 = 0$; $\varphi_u = 0$; $\Delta V/C = 0.02$; $\gamma = 1.2$.

An important parameter obtained from comparing the burning rate with the acoustic oscillations is the component of burning rate which is in-phase with the pressure oscillation. This in-phase component will be referred to as the response $\Re$. It can be extracted from the burning rate perturbations and nondimensionalized by a correlation procedure defined by

$$\Re = \int_0^{2\pi} W'P'd\omega t \Big/ \int_0^{2\pi} (P')^2 d\omega t \tag{5}$$

The response $\Re$ is a measure of the ability of a combustion process to drive acoustic oscillations. In linear analyses an $\Re$ greater than about unity usually implies unstable behavior. Whether the same criterion applies to distorted waves has not been rigorously established. Lacking analytical proof at this time, the criterion for the distorted waves considered in this analysis will be assumed the same as that for linear waves.

Exact solutions for the response $\Re$ were obtained by numerical techniques. The burning rate during one cycle of an assumed acoustic oscillation was computed by combining Eqs. (3) and (4) and the response $\Re$ was obtained by numerical integration of Eq. (5).

Results

The effect of varying the amounts of second harmonic content in the acoustic oscillations on response $\Re$ is shown in Fig. 1 (wave shapes are shown to indicate the distortion being considered). The response increases with the amount of second harmonic distortion when the distortion is relatively small. A maximum response is obtained where the second harmonic amplitude is 60% to 80% of the first harmonic. For any constant amount of second harmonic distortion, the response is a maximum for a pressure amplitude of about 0.02. One of the reasons for the decreased response at high amplitudes is a rapidly increasing average burning rate with amplitude. Large average rates reduce the relative size of any perturbation and reduce the response.

The lower curve in Fig. 1 ($p_2/p_1 = 0$) is the response for pure sinusoidal oscillations and provides a reference condition to gage the effect of distortion on response. The response for sinusoidal oscillations is relatively insensitive to the amplitude

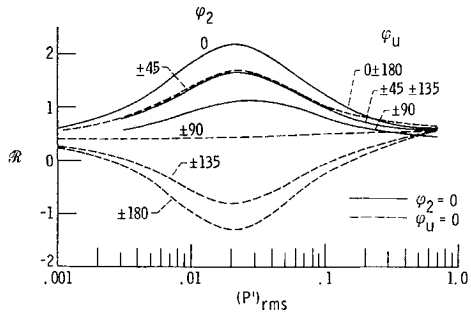

Fig. 2 Independent effect of second harmonic phase angle φ_2 and velocity phase angle φ_u on response. $\Delta V/C$ = 0.02; P_2/P_1 = 0.2; γ = 1.2.

of the oscillations. Compared to these sinusoidal oscillations waves distorted by second harmonics can amplify the response by a factor of 10. Although this large increase occurs for a relatively large amount of second harmonic content, the results demonstrate the extreme sensitivity of the process to harmonic distortion.

The amplification caused by wave distortion depends on both the phase relation between the first and second harmonic components (φ_2) and the phase relation between pressure and velocity (φ_u). Figure 2 shows the effect of both of these variables. Maximum response is obtained with in-phase properties ($\varphi_2 = 0$ and $\varphi_u = 0$). The response is much more sensitive to variations in the second harmonic phase angle than to the velocity phase angle. With velocity in-phase with pressure ($\varphi_u = 0$), second harmonic phase angle of $\pm 90°$ cancels all the distortion amplification and gives the response of sinusoidal oscillations. Phase angles beyond $\pm 90°$ cause a deamplification and in the extreme, give negative responses. The effect of velocity phase angle is much smaller. The response is above the sinusoidal value for all values of the velocity phase angle when harmonic components are in-phase ($\varphi_2 = 0$).

The drop vaporization process is velocity sensitive and the response of the process depends on this velocity sensitivity. The steady relative axial drop velocity or Mach number, $\Delta V/c$, controls this velocity sensitivity and its effect on the response is shown in Fig. 3. The amplification caused by wave distortion is negligible for relative axial Mach numbers above about 0.1 (about 500 fps in rocket combustors). However, relative velocities below this value typify many rocket combustors and amplification can become very large. Relative velocities generally increase with a decrease in the contraction ratio of rocket combustors. Instability should be less prevalent in low contraction ratio designs. Tests by Wanhainen et al.[5] confirm this deduction.

Some types of distortion found during acoustic resonance are adequately described by two harmonic components. Distortion, however, is more realistically characterized by a series of harmonic terms. A harmonic series which fitted the change in pressure wave shapes with amplitude in an experiment with strong traveling transverse acoustic resonance[4] was

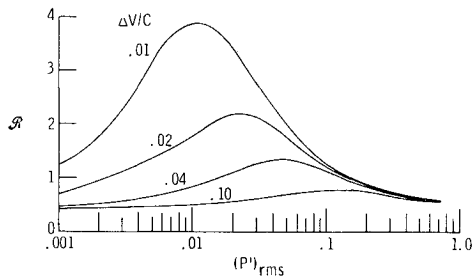

Fig. 3 Effect of relative axial drop velocity on response. p_2/p_1 = 0.2; φ_2 = 0; φ_u = 0; γ = 1.2.

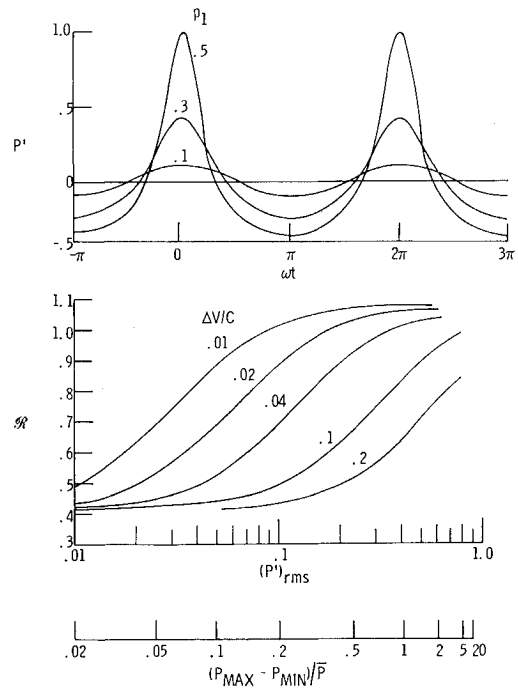

Fig. 4 Response for strong traveling transverse waves with multiple harmonic content, γ = 1.2.

found to be

$$P' = \sum_{n=1}^{\infty} (p_1)^n \cos n\omega t \tag{6}$$

Near the wall in the traveling mode the velocity is in-phase with pressure and acoustic properties can be approximated by

$$\rho' = (1/\gamma)P'; \quad u_\theta = (c/1.84\gamma)P' \tag{7}$$

The response and wave shape for such oscillations are shown in Fig. 4. The response generally increases with amplitude for a constant relative axial velocity up to a maximum response of about 1.08. The value is above that needed for instability in rocket combustors.

Figure 4 provides some insight as to why a disturbance above some finite value will cause a rocket combustor to be unstable. Increasing the size of the disturbance increases the harmonic distortion which amplifies the response. Above some level of disturbance, the amplification is sufficient to cause instability. The amplitude needed for instability ($\Re$ = 1 approx.) for the various axial velocities are comparable to the minimum amplitudes predicted by Priem and Guentert. Their results undoubtedly depended on the amplification caused by the wave distortion they observed.

Conclusions

This analysis shows wave distortion to be a crucial variable affecting combustion stability. It can amplify the response of a Reynolds number controlled process beyond that needed for unstable combustion.

The effect of wave distortion on the response of the combustion process is too large to be neglected in any stability analysis of a combustor. Quantitative agreement between experiment and analysis cannot be expected unless its effects are included. Progress toward unraveling some of the remaining apparent mysteries of combustion instability could be expected by directing more attention to the causes and effects of wave distortion.

It can also be concluded that harmonic distortion in combustors should be minimized because it is a cause of combustion instability. Selectively absorbing harmonic content and thereby altering wave shape may aid in controlling combustion

instability. Acoustic liners used in combustors selectively absorb certain frequency components that can alter wave shape. They may be most effective when they remove the second harmonic component of the basic oscillation.

References

[1] Heidmann, M. F. and Wieber, P. R., "Analysis of Frequency Response Characteristics of Propellant Vaporization," TN D-3749, 1966, NASA.

[2] Crocco, L. et al., "Nonlinear Aspects of Combustion Instability in Liquid Propellant Rocket Motors," AMS-SR-553g, NASA CR-72270, June 1967, Princeton Univ., Princeton, N.J.

[3] Priem, R. J. and Guentert, D. C., "Combustion Instability Limits Determined by a Nonlinear Theory and a One-Dimensional Model," TN D-1409, 1962, NASA.

[4] Heidmann, M. F., "Empirical Characterization of Some Pressure Wave Shapes in Strong Traveling Transverse Acoustic Modes," TM X-1716, 1969, NASA.

[5] Wanhainen, J. P., Feiler, C. E., and Morgan, C. J., "Effect of Chamber Pressure, Flow per Element, and Contraction Ratio on Acoustic-Mode Instability in Hydrogen-Oxygen Rockets," TN D-4733, 1968, NASA.

Transient Axisymmetric Bending Stress in an Infinite Cylindrical Shell at an Elastic Ring Stiffener

D. B. Longcope* and M. J. Forrestal†
Sandia Laboratories, Albuquerque, N. Mex.

An infinite, circular cylindrical shell containing an internal elastic stiffener ring is subjected to an axisymmetric, uniform, radial impulse. The bending stress in the cylindrical shell at the ring stiffener is calculated from the shell bending theory which neglects transverse shear deformation and rotary inertia. In Ref. 1, bending stresses for the special case where the stiffener ring was rigid were calculated on the basis of the shell bending theory and a shell theory, which included corrections for rotary inertia and transverse shear deformation. A comparison of the response data indicated that the effects of rotary inertia and shear deformation only influenced the very early time response, and that the shell bending theory was adequate for predicting the maximum bending stress.

Equations of Motion

For the circular cylindrical shell shown in cross section in Fig. 1, the equation of motion according to the shell bending theory, with the axial normal stress resultant taken as zero, is

$$(\partial^4 W/\partial X^4) + \alpha^2[W + (\partial^2 W/\partial T^2)] = (\alpha^2 cI/Eh)\delta(T) \quad (1a)$$

$$W = w/a;\ X = x/a;\ T = ct/a;\ c^2 = E/\rho;\ \alpha^2 = [12(1-\nu^2)a^2]/h^2 \quad (1b)$$

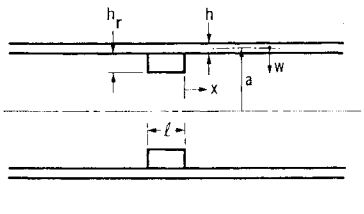

Fig. 1 Geometry of the problem.

Received September 14, 1970; revision received October 26, 1970. This work was supported by the U.S. Atomic Energy Commission.

* Staff Member, Exploratory Systems Development Department.

† Division Supervisor, Shock Simulation Department. Associate Fellow AIAA.

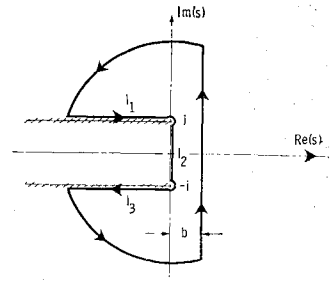

Fig. 2 Path of integration.

where w is the radial shell displacement; x is the axial coordinate; t is time; I is the specific impulse; $\delta(T)$ is the Dirac delta function; and a, h, ρ, E, and ν are the shell radius, thickness, density, Young's modulus, and Poisson's ratio, respectively.

The shell is infinite in either direction from the ring support, and the following boundary conditions for the shell are taken at the support

$$\partial W/\partial X = 0 \qquad \text{at } X = 0 \quad (2a)$$

$$\frac{\partial^3 W}{\partial X^3} + \frac{\alpha^2 L}{2}\left[(1+nK)W + (1+nM)\frac{\partial^2 W}{\partial T^2}\right] = \frac{\alpha^2 cIL}{2Eh}\delta(T) \qquad \text{at } X = 0 \quad (2b)$$

where

$$n = h_r/h;\ K = E_r/E;\ M = \rho_r/\rho;\ L = l/a \quad (2c)$$

and l, h_r, ρ_r, and E_r are the ring length, thickness, density, and Young's modulus, respectively. Symmetry requires that the slope of the shell vanishes at the ring stiffener and Eq. (2b) requires that the ring and shell displacements are equal at the ring-shell interface. It is assumed in the development of Eq. (2b) that the ring radius is equal to the shell radius a. Equation (2b) is essentially the equation of motion for a ring that includes the resistance of the shear forces of the shell; this is accounted for by the term $\partial^3 W/\partial X^3$. These shell boundary conditions are the same as those given in Ref. 2.

Solution

The bending stress in the shell at the ring stiffener is obtained by employing the Laplace transform method. The transform of Eq. (1a) with quiescent initial conditions is

$$\partial^4 \bar{W}/\partial X^4 + \alpha^2(1+s^2)\bar{W} = \alpha^2 cI/Eh \quad (3)$$

where $\bar{W}$ is the transform of W, and s is the transform variable. The transformed bending stress at the radially outer shell surface is given by

$$\bar{\sigma}_x^* = [Eh/2a(1-\nu^2)]\partial^2 \bar{W}/\partial X^2 \quad (4)$$

Equation (3) is solved subject to Eqs. (2a) and (2b) and the requirement that $\bar{W}$ is bounded as $X \to \infty$. The solution $\bar{W}$ is substituted into Eq. (4) and evaluated at $X = 0$ to give

$$\bar{\sigma}_x^* = \frac{\alpha cInM(a_0 + s^2)}{2a(1-\nu^2)(1+nM)(1+s^2)^{1/2}[b_0 + b_1(1+s^2)^{3/4} + s^2]} \quad (5a)$$

$$a_0 = K/M;\ b_0 = 1 + nK/1 + nM;\ b_1 = 2^{3/2}/\alpha^{1/2}L(1+nM) \quad (5b)$$

Thus the formal solution for the bending stress at the outer shell surface for $X = 0$ is

$$\sigma_x^* = \frac{1}{2\pi i}\int_{b-i\infty}^{b+i\infty} e^{sT}\,\bar{\sigma}_x^*\,ds \quad (6)$$

where b is a real, positive number.